

Exchange constants and spin waves of the orbital ordered, non-collinear spinel MnV_2O_4

R. Nanguneri, S. Y. Savrasov

Physics Department, University of California, Davis, California 95616, USA

We study the exchange constants of MnV_2O_4 using magnetic force theorem and local spin density approximation of density functional theory supplemented with a correction due to on-site Hubbard interaction U . We obtain the exchanges for three different orbital orderings of the Vanadium atoms of the spinel. We then map the exchange constants to a Heisenberg model with single-ion anisotropy and solve for the spin-wave excitations in the non-collinear, low temperature phase of the spinel. The single-ion anisotropy parameters are obtained from an atomic multiplet exact-diagonalization program, taking into effect the crystal-field splitting and the spin-orbit coupling. We find good agreement between the spin waves of one of our orbital ordered setups with previously reported experimental spin waves as determined by neutron scattering. We can therefore determine the correct orbital order from various proposals that exist in the literature.

PACS numbers: 71.20.-b, 71.45.Gm, 71.70.Ej, 71.70.Gm

I. INTRODUCTION

Transition metal oxides (TMO) are a class of solid-state materials that exhibit a rich variety of physical phenomena¹. Among them, magnetic cubic spinels AV_2O_4 have recently attracted much attention due to geometrically frustrated corner sharing tetrahedral network formed by the V atoms (also known as a pyrochlore lattice)². An interesting example is represented by MnV_2O_4 which is the spinel having additional magnetic Mn ions. It exhibits an orbital ordering (OO) that occurs at finite T as a thermal phase transition: At room temperature, single crystalline MnV_2O_4 is a cubic paramagnet (PM) where Mn sites occupy the centers of oxygen tetrahedra (MnO_4 units), while V sites occupy the centers of oxygen octahedra (VO_6 units). As T is lowered there is a magnetic phase transition at $T_F = 56$ K from the high- T PM phase to a cubic ferrimagnetic (FEM) phase, with the Mn and V moments anti-aligned. When T is lowered further below $T_S = 53$ K there is a second transition to a tetragonal, non-collinear FEM with trigonal distortion of VO_6 octahedra and orbital ordering of $V^{3+} 3d^2$ electrons³. The structural transition and orbital ordering occur together via the Jahn-Teller effect, which states that when there is an orbital degeneracy, as in the V atoms, structural distortion occurs to remove the degeneracy and lower the total energy. The orbital ordering is also accompanied by a reduction of the V magnetic moments due to the formation of the electron orbital moment (finite orbital angular momentum). The orbital moment, $m_o \approx 0.34$, is anti-aligned with the spin moment, $m_s \approx 1.65$, giving the total moment of $m \approx 1.31$ ³. The reduced value of V moment has been reproduced by an earlier first-principles work in Ref. 4, and is explained by the spin-orbit coupling (SOC) on the V $3d^2$ which generally favors anti-alignment of spin and orbital angular momenta for T below the energy scale of SOC².

The local tetrahedral and octahedral coordination of

the Mn and V sites, respectively, results in lifting the degeneracy of their five $3d$ orbitals known as crystal-field (CF) splitting. From group-theoretical considerations⁵, the 5-fold degenerate $3d$ level is split into a 2-fold degenerate e_g and a 3-fold degenerate t_{2g} manifold. For tetrahedrally coordinated Mn, the e_g is lower in energy as compared to the t_{2g} , whereas for octahedrally coordinated V, the $e_g - t_{2g}$ splitting is opposite. There is also Hund's rule splitting of up and down spins, which is greater than the CF splitting. In the stoichiometric crystalline environment, Mn has an outer shell high-spin $S = 5/2$ configuration of $3d^5$ and a valence of +2: all the up-spin $3d$ orbitals are occupied, and the down spin ones are empty. V has a valence of +3, an outer shell configuration of $3d^2$, and total spin $S = 1$: in this case, 2 electrons must occupy the 3 t_{2g} xy , yz , zx orbitals. In the high temperature cubic phase, these latter three are degenerate, while in the low temperature tetragonal phase, where the unit cell is slightly compressed along the c -axis, the xy is lowered in energy while yz , zx remain degenerate. Thus, in the tetragonal (low- T) phase, one electron on V occupies the xy , and the second electron has the freedom to occupy either yz , or zx . The total angular momentum of the Mn atom is quenched, $L = 0$, due to the equal occupation of all the z -axis projections of L , which makes the total projection $L_z = 0$. On the other hand, the total angular momentum of V is not fully quenched: The partial occupation of the yz and zx gives an effective total angular momentum $L = 1$ for V. The fact that $L \neq 0$ implies that there maybe non-negligible effects of SOC in the V atoms². Further, this is a hint that the yz and zx form complex linear combinations of one-electron states, since only such a complex state can carry non-zero angular momentum. The freedom of the second electron of V to occupy yz , zx , or some linear combination of the two gives rise to the possibility of long-range orbital order in the low temperature phase.

The number of possibilities for the occupation of the second electron is infinite, due to the infinite different ways in which one can form linear combinations of the yz ,

and zx orbitals. However, two simple choices exist and both have been studied theoretically in mean field models. One is the Antiferro-Orbital Order (AFOO) with alternate occupation of the yz and zx along the c -axis, i.e.: the same orbital is occupied in a given ab -plane but the other orbital is occupied in the adjacent planes above and below^{3,6,7}, as shown in Fig. 1(a). This order has the point-group symmetry $I4_1/a$. The second is the Ferro-Orbital Order (FOO) where the same orbital is occupied on all V-atoms⁸, giving the symmetry group $I4_1/amd$, as shown in Fig. 1(b). In particular, in the latter orbital order the linear combination can be complex, in which case there will be a non-zero orbital angular momentum and a magnetic moment associated with it⁹. Spin-orbit coupling can stabilize the finite orbital moment, since the energy is lower for anti-parallel alignment of \vec{L} and \vec{S} .

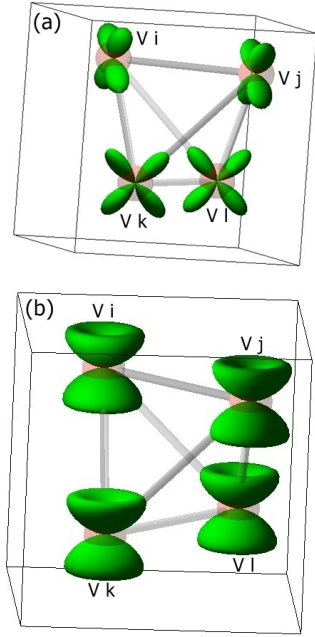


FIG. 1. (a) Schematic illustration of the initial real antiferro-orbital order of the type I (AFOO I) with $L = 0$ on the four corners of the V tetrahedron. The lower and upper horizontal bonds are in the ab plane. The red spheres are the V atoms. The lower ab plane has yz orbitals occupied on all V, while the upper ab plane has zx occupied on all V. (b) Schematic illustration of initial ferro orbital order on all four corners of the V tetrahedron where an electron occupies the same real linear combination of yz and zx on all V sites. Note that the self-consistent solution breaks this symmetry and results in an electron occupying alternately $\psi_+ = (\psi_{yz} + \psi_{zx})/\sqrt{2}$ and $\psi_- = (\psi_{yz} - \psi_{zx})/\sqrt{2}$ along the c -axis. We refer to this order as antiferro-orbital order of type II (AFOO II). The indices i, j, k, l denote the inequivalent V sites in the FCC primitive cell.

In both of the above proposals, trigonal distortion of the VO_6 octahedra is not taken into account, but it is known to be large in MnV_2O_4 as compared to other vanadates. This distortion lifts the residual degeneracy

between yz , zx , and the degeneracy of the e_g manifold. In this case, the above OO proposals are not necessarily correct as these assume degeneracy between the yz , zx orbitals. The trigonal distortion could possibly be due to the Jahn-Teller effect^{10,11} and has indeed been observed in a previous first-principles work⁴ that used local spin density approximation (LSDA) of density functional theory (DFT)¹² supplemented by the correction due to on-site Hubbard interaction U ¹³ for correlation strengths $U > 2$ eV. In that work, in addition to a tetragonal relaxation (compression) along the c -axis, structural relaxation of the O positions is performed and a trigonal distortion of the VO_6 octahedron with a concomitant lowering of symmetry from $I4_1/amd$ to $I4_1/a$ is found. In this relaxed structure, due to the low symmetry at the V sites, all five $3d$ orbitals get mixed and the resulting five one-electron eigenstates of the on-site V block of the full LSDA+U Hamiltonian have different eigenenergies. By projecting the converged density onto an atomic orbital basis using so called non-linear muffin-tin orbital (NMTO) downfolding¹⁴, the authors of Ref. 4 find a different electron occupation order from the ones proposed above, namely, the first electron occupies the lowest energy eigenstate, and the second occupies the next higher energy eigenstate, which is the same on all V sites, but rotated alternatively by 45° along the ab -chains due to the staggered trigonal distortion. Thus, the same orbitals are occupied on all V sites, akin to the ferro-orbital order, but nevertheless the symmetry is the $I4_1/a$ expected of antiferro-orbital order due to the trigonal distortion.

The low- T magnetic excitations of the compound have been mapped along high-symmetry directions using inelastic neutron scattering^{3,15}. At the Γ point, these excitations are gapped for the acoustic modes, indicating the presence of single-ion anisotropy, which essentially occurs due to the interplay between SOC and crystal-fields¹⁶. In Ref. 15, the authors start with a nearest-neighbor Heisenberg Hamiltonian including the anisotropy term and calculate spin-wave spectra and corresponding eigenmodes using linear spin-wave theory (LSWT) for the non-collinear, tetragonal phase. By fitting the spectrum to inelastic neutron scattering data (performed at sample temperature of 5 K), they were able to determine the exchange couplings between Mn-V, V-V in ab -plane, and V-V between ab -planes along the c -axis. They find all exchanges to be AFM with the following values:

- $J_{Mn-V} = -2.82$ meV
- $J_{V-V}^{ab} = -9.89$ meV
- $J_{V-V}^c = -3.08$ meV

The interplanar coupling between V atoms, J_{V-V}^c , along the c -axis is unusually large for AFOO because such an alternate orbital occupation in the vertical direction would yield negligible orbital overlap, and would also be ferromagnetic (wrong sign) by the Goodenough-Kanamori rules¹⁷. The alternate proposal, FOO, would

be consistent with these results, but would have the wrong symmetry, $I4_1/amd$. The symmetry group of this spinel vanadate has been established conclusively as $I4_1/a$ by a synchrotron x-ray study⁷ which supports AFOO, but contradicts with the large value of J_{V-V}^c . A possible resolution of this puzzle is that trigonal distortion has been ignored in these simple proposals. With trigonal distortion, we expect a more complex orbital ordering which has the requisite symmetry $I4_1/a$ and would give the observed (or fitted) J_{V-V}^c along the c -axis¹⁵. This is exactly what has been found in the ab-initio work of Ref. 4. Their physical picture has also received some support by a recent ⁵¹V NMR work of Ref. 18 and by analytical model of Ref. 19.

In this work, we report our study of MnV_2O_4 based on the LSDA+U method and using linear muffin-tin orbital (LMTO) basis set to solve the electronic structure problem^{20,21}. We calculate the pair-wise interatomic magnetic exchange interactions (J) between all magnetic atoms using linear response theory and magnetic force theorem^{22,23}, including the single-ion anisotropies (D) for Mn and V found by the exact diagonalization procedure¹⁶. We then use the obtained J and D as parameters in a Heisenberg Hamiltonian with anisotropy to derive the spin-wave spectra in a semiclassical approximation. We explore three initial orbital ordering scenarios: [1] Antiferro, [2] Ferro, and [3] Complex ferro + SOC in the density matrix of the $3d$ shell of V to see how they affect the obtained exchange interactions. We also performed non-collinear magnetic electronic structure calculations. Although we do not relax the structure, and hence do not incorporate trigonal distortion, we find a good fit between our theoretical spin-waves for the SOC complex ferro-orbital order and the experimental spin waves. We conclude that trigonal distortion is a *higher-order consequence* of the orbital order and of electron correlations, and as such has a negligible effect on the exchange constants. Since LSDA+U has many solutions, we make the argument that our converged charge density maybe as good as the one found in Ref. 4 for the purposes of calculating the exchange interactions. We can further justify this point of view using the approach of Kugel-Khomskii (KK) models, in which both spin and orbital degrees of freedom are dynamical variables coupled to each other (these models are derived from multi-orbital Hubbard models using second-order perturbation theory)¹⁰. Simultaneous spin and orbital order is obtained by minimizing the mean-field total energy of the KK Hamiltonian with respect to the local orbital and spin order parameters. There is not yet any lattice distortion (indeed, the lattice is not a dynamic variable in the KK Hamiltonian), however, with a non-zero electron-phonon interaction (which is generically present in all materials) any orbital order (or polarization) will automatically lead to a lattice distortion *as a consequence*^{10,24}.

Along these lines, an example of orbitally driven lattice distortions is discussed in the context of the spinels $MgTi_2O_4$ and $CuIr_2S_4$ by Khomskii and Mizokawa in

Ref. 25. These authors consider orbital ordered Peierls distortion and spin singlet formation along chains of Ti and Ir atoms. The lattice distortion then follows as a consequence.

Our paper is organized as follows. We begin with a discussion of the proposed orbital orders and their electronic structures in Section II. We present our results for exchange interactions and comparisons with experiment in Section III. We end with the conclusions in Section IV.

II. PROPOSED ORBITAL ORDERS AND THEIR ELECTRONIC STRUCTURES

We have done LSDA+U calculations to model the electronic structure for all three thermodynamic phases of MnV_2O_4 . We describe our results in the following subsections for the $T = 0$ phase only since this is the phase which exhibits orbital ordering and non-collinear magnetism. Our results for the other finite- T phases may be found in Ref. 26. For the magnetic phases we use the same values of U and J for both Mn and V correlated $3d$ shells. The use of the same U on Mn and V is justified because these elements have atomic numbers 25 and 23, and are thus expected to have similar interaction strengths⁴. The Coulomb and exchange parameters in the solid state are generally screened, and hence reduced by a considerable amount from their bare atomic values²⁷. The structural parameters for all three phases are taken from experiment³: In the cubic phase, the lattice constant is 16.0746 a.u., and in the tetragonal phase it is 16.12 a.u. with a small tetragonal distortion ratio of $\frac{c}{a} = 0.98$.

The non-collinear orbital ordered phase occurs when the temperature is reduced below $T_S = 53$ K. This phase transition results simultaneously in: [1] a structural transition from cubic to tetragonal; [2] the canting of V moments from a *collinear* ferrimagnetic (FEM) to a $\mathbf{q} = 0$ *non-collinear* FEM spin order with non-zero components in the ab -plane; and [3] a long-range orbital order in the V t_{2g} manifold. We model the electronic structure of this phase using LSDA+U method with $U = 5$ eV and $J = 1$ eV, but starting the self-consistency loop after imposition of the initial orbital order(s) in the Hubbard-U density matrix (further described below), along with tetragonal distortion and two different magnetic configurations: [1] *collinear*, as in the intermediate phase, and [2] *non-collinear*, which is in fact the correct magnetic order for this phase. The converged charge density for the low- T *collinear* calculation was used as the initial charge density for the correct low- T *non-collinear* calculation. The orbital order that is finally obtained after reaching the self-consistency is taken to be the correct metastable solution within this approximation and specified initial condition(s).

We initialize the V $3d$ density matrix to a particular orbital order by specifying orbital occupation numbers in the atomic basis. This means we initially spec-

ify only the diagonal components (occupation numbers) $\langle n_{xy\uparrow} \rangle$, $\langle n_{yz\uparrow} \rangle$, $\langle n_{zx\uparrow} \rangle$ of the density matrix for all four V atoms' 3d shells and set the off-diagonal elements to zero. The full complex density matrix in the atomic basis is $\langle n_{m\sigma, m'\sigma'} \rangle$ (where m, m' and σ, σ' are the 3d orbital and spin indices respectively) and includes off-diagonal components as well. As a result of the electron-electron interactions, during the self-consistent cycle non-zero off-diagonal components of the density matrix develop (since the interactions mix the single-particle 3d orbitals at the Hartree-Fock (HF) mean-field level). This means the true occupied orbitals are some linear combination of the atomic basis functions. After convergence is reached, the final density matrix, which is no longer diagonal in the $(m\sigma, m'\sigma')$ basis is diagonalized. The resulting eigenvectors and eigenvalues give the 'correct' single-particle HF wave functions and their occupation numbers respectively. In the basis of these eigenfunctions, the density matrix is once again diagonal, and its non-zero entries signify the true orbitals which are occupied within the mean-field approximation of LSDA+U. We are thus able to identify the orbital ordering that results after convergence is attained. We describe the final orbital orders below for the *collinear* magnetic solutions only, since we find that the electronic structures, and therefore the orbital orders, of the *non-collinear* configurations are not significantly different from the corresponding *collinear* ones as discussed below.

A. Anti-Ferro Orbital Order I: $I4_1/a$ symmetry

In the low- T orbitally ordered phase, the tetragonal distortion occurs to break the degeneracy of the t_{2g} in both V and Mn. There is no orbital freedom to place the electrons in the Mn 3d. In the V, the energy of xy gets lowered, so the first electron occupies xy . The second electron then has the freedom to occupy the remaining degenerate orbitals yz or zx . Figure 1(a) shows the initial orbital occupations with $I4_1/a$ symmetry. In this scenario, the second electron of V occupies either yz or zx alternately along the c -axis (antiferro OO), and the same orbital within each ab plane^{3,7}. (Each V chain within an ab plane has the same orbital occupied.) The final converged density matrix of the V 3d subspace shows that this initial order persists until convergence, although some small off-diagonal components do emerge. We label this order 'AFOO I'.

The *collinear* spin fat bands of V t_{2g} electrons are shown in Fig. 2(a), and the same for *non-collinear* spins in Fig. 2(b). The occupations of the $t_{2g}\uparrow$ bands, as shown by the partial characters, reflects the converged orbital order, as well as the FEM spin configuration. We also find that imposition of orbital order opens a gap of about $E_{\text{gap}} = 1.67$ eV at the Fermi level leading to an insulator state. The qualitative features of the band structure and partial characters does not change upon canting the V moments to the non-collinear configura-

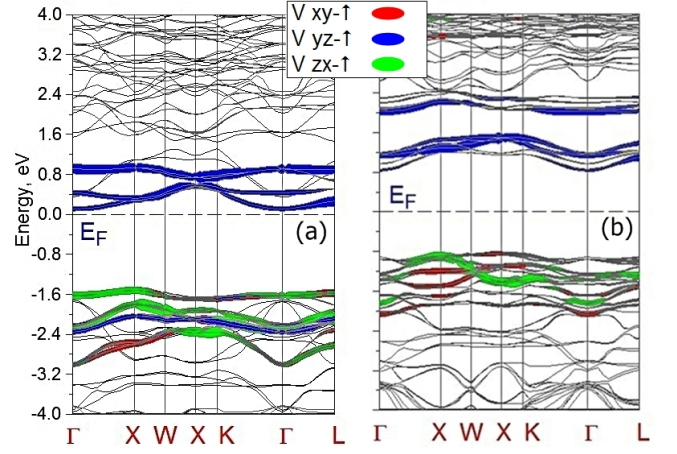


FIG. 2. (a) The V $t_{2g}\uparrow$ bands for $U = 5$ eV in the low- T tetragonal phase with a *collinear* ferrimagnetic spin configuration and real antiferro-orbital order of the type I (AFOO I) as discussed in text. (b) Bands for the same setup as in (a) but with a *non-collinear* ferrimagnetic spin configuration. In both panels, the partial characters of the $xy\uparrow$, $yz\uparrow$, $zx\uparrow$ orbitals are for the sublattice i, j V atoms. We see that due to the orbital ordering, the $zx\uparrow$ is occupied while the $yz\uparrow$ is mostly unoccupied. The occupations of these two orbitals are reversed for the sublattice k, l V atoms on the adjacent parallel ab planes along the c -axis. The sublattice indices are defined in Figs. 1, 5. There is a band-gap of $E_{\text{gap}} = 1.67$ eV.

tion: The band gap remains robust and the phase is still insulating.

B. Anti-Ferro Orbital Order II: $I4_1/a$ symmetry

The next simplest *initial* order has the second t_{2g} electron occupying the same real linear combination of yz and zx on all V sites, with equal weight for both orbitals, see Fig. 1(b). This initial order has $I4_1/amd$ symmetry. The real linear combination implies that the orbital angular momentum is zero, $L = 0$. We implement this by setting the initial mean occupations: $\langle n_{xy} \rangle = 1$, $\langle n_{yz} \rangle = \langle n_{zx} \rangle = 1/2$ (ferro OO), and the off-diagonal elements to be zero. For this setup, the initial order *does not* persist until convergence is reached. Instead, there are significant non-zero off-diagonal elements, on the same order as the occupied diagonal elements, in the final density matrix. Upon diagonalizing this final matrix, the orbital order we get has the second electron occupying alternately $\psi_+ = (\psi_{yz} + \psi_{zx})/\sqrt{2}$ and $\psi_- = (\psi_{yz} - \psi_{zx})/\sqrt{2}$ along the c -axis, which again has the same $I4_1/a$ symmetry considered in the preceding subsection. Thus, we start with an orbital order with $I4_1/amd$ symmetry, but the self-consistent solution breaks certain discrete symmetries and results in an order with $I4_1/a$ symmetry. We thus label this order 'AFOO II'.

The *collinear* spin fat bands of V t_{2g} and e_g are shown in Fig. 3(a), and the same for *non-collinear* spins in

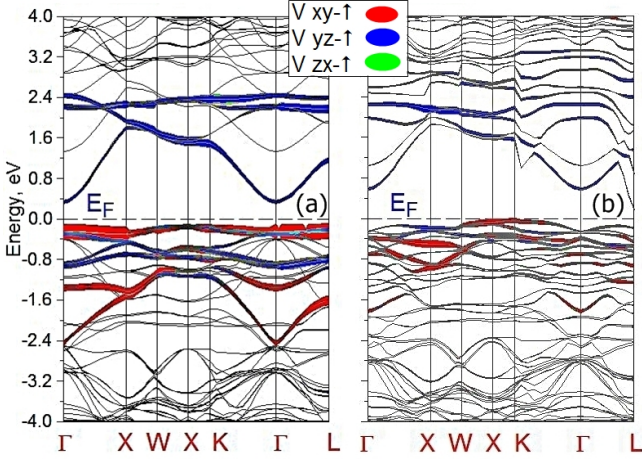


FIG. 3. (a) The V $t_{2g-\uparrow}$ bands for $U = 5$ eV in the low- T tetragonal phase with a *collinear* ferrimagnetic spin configuration and real antiferro-orbital order of the type II (AFOO II) as discussed in text. (b) Bands for the same setup as in (a) but with a *non-collinear* ferrimagnetic spin configuration. In both panels, the partial characters of the $xy-\uparrow$, $yz-\uparrow$, $zx-\uparrow$ orbitals are for the sublattice i, j V atoms. Note that the yz and zx partial characters have nearly identical dispersions due to their equal weight in the occupied orbital. There is again a band-gap for this orbital-order too.

Fig. 3(b). Qualitative features of the band structures do not change significantly between the collinear and non-collinear spin configurations. In both plots, the occupations and dispersions of the yz and zx bands are nearly identical since these orbitals contribute equal weights to the true orbitals, although their relative signs in the linear combinations might differ in these depending on the particular V atom. We also find an insulating band-gap, which in this case is smaller than for ‘AFOO I.’

C. Complex Ferro Orbital Order: $I4_1/amd$ symmetry

The last OO has one electron in xy as before, and the second electron in the spherical harmonic $L_z = -1$, $S_z = +1/2$ state, which is a complex linear combination of yz and zx , on all V sites. This is an initial ferro-orbital order, but with SOC switched on and non-zero orbital angular momentum. The initial density matrix configuration persists until convergence. This calculation is carried out using LSDA+U+SO. This scenario is also illustrated by Fig. 1(b), except that each V atom now carries a non-zero orbital angular momentum of magnitude one due to the complex linear combination; hence, there is a uniform orbital order on all V atoms with $L = 1$ in the $3d$ density matrix. The reason for choosing the opposite z -projections for L and S is that spin-orbit interaction lowers the energy for such a setup, compared to the case of having the same sign for both z -projections.

In Fig. 4(a) we present the band structure of MnV_2O_4 ,

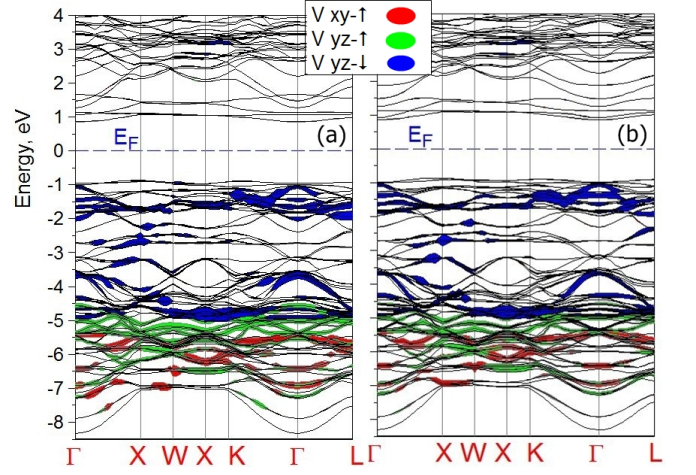


FIG. 4. (a) The V $t_{2g-\uparrow}$ band characters for the low- T tetragonal phase with a *collinear* FEM spin configuration and complex ferro-orbital order with spin-orbit coupling (SOC-FOO) as discussed in text. (b) Bands for the same setup as in (a) but with a *non-collinear* ferrimagnetic spin configuration. In both panels, the partial characters of the $xy-\uparrow$, $yz-\uparrow$, $yz-\downarrow$ orbitals are for the sublattice i, j, k, l V atoms. There is a band-gap of $E_{\text{gap}} = 1.76$ eV. The V $xy-\downarrow$ band lies above E_F , the $zx-\uparrow$ bands coincide with the $yz-\uparrow$ so we omit it, and finally the $zx-\downarrow$ bands are in the same energy region as the $yz-\downarrow$ so again we omit it.

for the *collinear* magnetic configuration, with the V $t_{2g-\uparrow}$ partial characters of the SOC uniform orbital order. We find that the V $t_{2g-\downarrow}$ and e_g characters are above the E_F as expected. For Mn, all the $3d-\downarrow$ are below E_F , while the $3d-\uparrow$ are above. There is a band gap of 1.76 eV. Within LSDA+U a half-metallic solution was found in Ref. 4, with only the \uparrow -spin bands of V atoms crossing the E_F level, a result which we have also confirmed²⁶. Our result is that inclusion of SOC in LSDA+U opens a band gap, signaling a half-metal-to-insulator transition as the SO coupling parameter is switched on. Since we argue that the uniform complex ferro order is the correct orbital order based on exchange constant calculations, we predict a half-metal-to-insulator transition to occur in single crystalline MnV_2O_4 as the temperature goes below T_S . In Fig. 4(b) we present the corresponding band structure of the *non-collinear* magnetic configuration for this order, with the partial characters of V t_{2g} shown. We find that the Mn atoms carry no orbital moment, but the V atoms have an orbital moment $m_o = 1.03$. The spin moments are $m_s = 4.33$ for Mn, and $m_s = 1.71$ for V. Since the spin and orbital moments are antiparallel due to SOC coupling, the total moment for V is $m \approx 0.7$ in this phase.

We note for comparison that Ref. 4 also finds a uniform (same) orbital occupied on all V sites, except that they relax the structure to obtain trigonal distortion of the VO_6 octahedra, and hence a 45° rotation of the second electron’s t_{2g} orbital on alternate V atoms of the ab -plane V chains. We do not have a trigonal distortion

in our setups, but we do find that the resulting exchange interactions correctly describe the spin-wave excitations of the low- T *non-collinear* phase (see below). This gives us a confidence that trigonal distortion has only a minimal influence on the magnetic exchange interactions, and that our LSDA+U+SO orbital order is equally good for the purpose of computing these interactions. For reference, we label this order as ‘SOC-FOO’.

III. RESULTS FOR EXCHANGE INTERACTIONS

Here we outline the spin-wave model, the ground state spin configuration, and present the results for our calculated exchange constants J and single-site anisotropy parameters D . Our obtained spin wave spectra of MnV_2O_4 and comparisons with the neutron scattering experiments

are also given.

A. Spin Wave Model

The parameters of the model are: [1] the exchange constants J derived from the LSDA+U(+SO) converged charge densities using linear response theory and the magnetic force theorem^{22,23}, and [2] the single-ion anisotropy parameters D calculated using an exact-diagonalization atomic multiplet procedure¹⁶. We input these parameters into the Heisenberg model Hamiltonian with anisotropy terms, minimize the classical energy to find the stable ground state configuration, and calculate the spin-wave excitation spectra. The model Hamiltonian is:

$$H_{\text{spin}} = - \sum_{\langle ij \rangle} J_{ij} \vec{S}_i \cdot \vec{S}_j - \sum_{\langle ik \rangle} J_{ik} \vec{S}_i \cdot \vec{S}_k - \sum_{\langle il \rangle} J_{il} \vec{S}_i \cdot \vec{S}_l - \sum_{\langle jk \rangle} J_{jk} \vec{S}_j \cdot \vec{S}_k - \sum_{\langle jl \rangle} J_{jl} \vec{S}_j \cdot \vec{S}_l - \sum_{\langle kl \rangle} J_{kl} \vec{S}_k \cdot \vec{S}_l \\ - J_{\text{Mn-V}} \sum_{\langle (p,q)(i,j,k,l) \rangle} (\vec{S}_p + \vec{S}_q) \cdot (\vec{S}_i + \vec{S}_j + \vec{S}_k + \vec{S}_l) - \sum_{\langle pq \rangle} J_{pq} \vec{S}_p \cdot \vec{S}_q + \sum_{x=i,j,k,l,p,q} \vec{S}_x \cdot \vec{D}_x \cdot \vec{S}_x. \quad (1)$$

The subscripts on the J label the four inequivalent V sublattices, i, j, k, l, and two inequivalent Mn sublattices, p, q. The $J_{\text{Mn-V}}$ is taken outside the summation because it has the same value for all pairs of Mn and V atoms. All the J couplings are between nearest-neighbor atoms of two different sublattices, and each pair is counted only once in the summation over all sites. We ignore the next-nearest-neighbor couplings because we found them to be much smaller in magnitude.

B. Spin Configuration

The low- T spin structure is non-collinear for V atoms, and collinear for Mn atoms with respect to the c -axis. The pyrochlore lattice on which the V atoms sit is geometrically frustrated for nearest-neighbor isotropic ($J^{ab} = J^c$) AFM exchange. The frustrated pyrochlore interactions mean that there could be a macroscopic ground state degeneracy. But this frustration is partially relieved in the low- T phase by the presence of additional nearest-neighbor exchange interactions with Mn atoms, tetragonal distortion, and orbital ordering. The last one has the effect of making the V-V AFM exchange anisotropic: $J^{ab} \neq J^c$. It is well-known that the orbital or magnetic degeneracy can be lifted by the coupling of these degrees of freedom with the lattice via the Jahn-Teller effect^{1,11}. The ground-state spin configuration selected by the system in the low- T phase is non-collinear due to the combined effect of the frustration and coupling

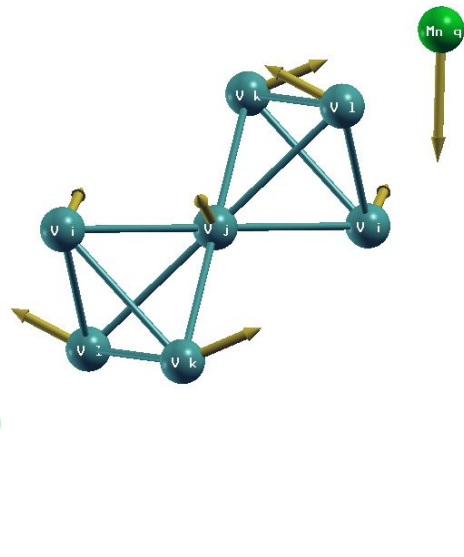


FIG. 5. The $T = 0$ non-collinear spin configuration of the V spins from Ref. 3.

of the V spins to Mn spins, V t_{2g} orbitals, and the lattice. In this structure, the V-atom spins develop components in the ab plane perpendicular to each other. The amount of canting away from the c -axis can be characterized by a single canting angle θ . Given the values of all J and D in Eq. 1, one can find the angle θ as a function of J and D that will minimize the classical ground-state energy

of the configuration (derivation given in Ref. 26):

$$\theta = \arccos\left[-\frac{3J_{\text{Mn-V}}S_{\text{Mn}}}{(D_V^z - D_V^{x,y} - 2J_{\text{V-V}}^c - 2J_{\text{V-V}}^{ab})S_V}\right]. \quad (2)$$

The non-collinear spin configuration that achieves this energy minimum is shown in Figure 5²⁸.

C. Exchange Constants

In Table I we present the J parameters that we calculate using LSDA+U method and magnetic force theorem. As the method computes the exchange constants in reciprocal space, we Fourier transform them and show only nearest-neighbor exchange interactions between atoms of each sublattice. For the spinel structure, any of nearest-neighbor pairs always belongs to a different sublattice. The values of $J_{\text{V-V}}$ for no orbital order and $U = 0$ eV are the same for all V-V pairs; but when $U = 5$ eV, there is a tendency for anisotropy to develop: the in-plane $J_{\text{V-V}}^{ab}$ becomes unequal from the out-of-plane $J_{\text{V-V}}^c$. This is one reason in support of our earlier argument that the anisotropy in the $J_{\text{V-V}}$, and the orbital ordering which causes it, are both interaction driven. When there is an orbital order, $J_{\text{V-V}}$ is different along the ab V chains and between the chains (along the c -axis), as expected. This is true even for the case of the uniform orbital orders, because the exchange matrix elements of the Coulomb operator will be different within the ab plane and between the planes, as can be seen from the shapes of the occupied orbitals in Fig. 1(a,b).

D. Single-Ion Anisotropy

The calculation of single-ion anisotropy requires first the total energies of the interacting atomic shell in a crystal-field environment along with the spin-orbit coupling. The method for its computation is described in Ref. 16 and 26, so here we merely present our results. The input parameters used in the total energy calculation are: the SOC parameter 0.15 eV, and Slater integrals $F_0 = 5.0$ eV, $F_2 = 7.6$ eV, $F_4 = 4.7$ eV. We then vary the direction of the magnetic moment by applying a small external magnetic field. The CF levels have the following values: the energies of yz and zx are both set to the reference value of 0.0 eV. The e_g level is varied from 0.2 eV to 1.0 eV in steps of 0.2 eV; and the xy level has the energies -0.024 eV, -0.016 eV, -0.008 eV, 0.0 eV. This gives a set of 20 different CF configurations. The $E_{xy} = E_{yz/xz}$ represents cubic CF, and $E_{xy} \neq E_{yz/xz}$ represents tetragonal CF.

The total atomic shell energies thus obtained are fitted to a parabolic function of the polar angle θ representing moment orientation, centered at $\theta = 0$ in the case of z -axis anisotropy, and centered at $\theta = \pi/2$ in the case of x/y -axis anisotropy. The results of the parabolic fit that

best match the experimentally known D values are given in Table II for both the V $3d^2$ and Mn $3d^5$ shells.

The easy axis for Mn is $z(c)$ -axis, and for V it is either x or y . The easy axis always has a negative anisotropy parameter, which means the energy is lowered when the spin projection along the easy axis is maximized. For Mn, the spin projection along z tends to be maximized. However, V also has a positive anisotropy parameter along the z -axis. So, V spin projection likes to be maximized along y , and minimized along z ¹⁵. Thus, the V spin moment has a tendency to be in a non-collinear direction with respect to the z -axis. Our anisotropy computation is able to reproduce these signs as well as magnitudes for Mn ($3d^5$) and V ($3d^2$) shells.

Looking at the anisotropy fit values we see that the value of Mn anisotropy reported in Ref. 15 are obtained for $E_{xy} = -0.016$ eV, $E_{e_g} = 1.0$ eV, namely $D_{\text{Mn}}^z = -0.1123$ meV, which is similar to the literature value. For our fitted values of V anisotropy, we do not find such a close match, but there are several CF values which give the anisotropy of Ref. 15 up to the correct sign and order of magnitude. For example, $E_{xy} = -0.024$ eV, $E_{e_g} = 0.4$ eV give $D_V^z = 7.34$ meV, and $D_V^{x,y} = -4.056$ meV, which can be compared to $D_V^z = 2.79$ meV, and $D_V^{x,y} = -4.04$ meV of Ref. 15. One reason why our calculated D_V^z parameter differs by a large amount from the experimental value is because we have to tune the CF energy levels to simultaneously match two different single-ion anisotropies, and it was not possible to get them both to match the experimental D values of V.

E. Spin-Wave Spectra

We developed a code to compute the linear spin wave spectra for the non-collinear spin configuration. The program takes as an input our computed values of J and D . We first find the ground state which will in general be a non-collinear configuration with the spins pointing along the local quantization axis as given by θ in Eq. 2. We second find the Heisenberg equations of motion, and numerically diagonalize the resulting system of linear equations. The resulting spin-wave spectra are plotted in Fig. 6(a) for the SOC uniform orbital order, along with the experimental spin waves. We find that the spin waves obtained from the J and D values of the SOC ferro-orbital order matches well with experiment. We also note that the lower two modes are due to the oscillations of Mn spins: The lower energy being the symmetric mode, and the higher energy the anti-symmetric mode¹⁵. The upper four modes are oscillations of the V spins¹⁵.

For comparison, we also show the spin waves for the other orbital orders *do not* match well with the experimental data. The model parameters for these orbital orders do give a reasonable spin canting angle when using Eq. 2, but the upper branches of the spin waves corresponding to the V oscillations are too high in energy and have a larger band-width in these plots (due to consid-

meV	No OO $U = 0$ eV	No OO $U = 5$ eV	AFOO-I $U = 5$ eV	AFOO-II $U = 5$ eV	SOC-FOO $U = 5$ eV	Expt. ¹⁵
J_{ii}	-2.72	0.136	0.3264	-0.04488	0.1496	-
J_{V-V}^{ab}	-20.4	-21.76	-14.96	-19.04	-11.56	-9.89
J_{V-V}^c	-20.4	-18.36	-3.536	-7.072	-2.72	-3.08
J_{Mn-V}	-10.2	-2.992	-5.44	-5.44	-4.76	-2.82
J_{pq}	1.2	2.167	2.72	2.72	2.72	-
J_{pp}	-0.476	0.204	0.204	0.272	0.272	-

TABLE I. Calculated exchange constants in meV for the *collinear* ferrimagnetic configurations and imposing various orbital orders. The last two columns list our theoretical J s for the spin-orbit coupled ferro-orbital order (SOC-FOO) and experimental J 's from Ref. 15 respectively. The experimental J 's match the SOC-FOO J 's better than for the other theoretical J 's.

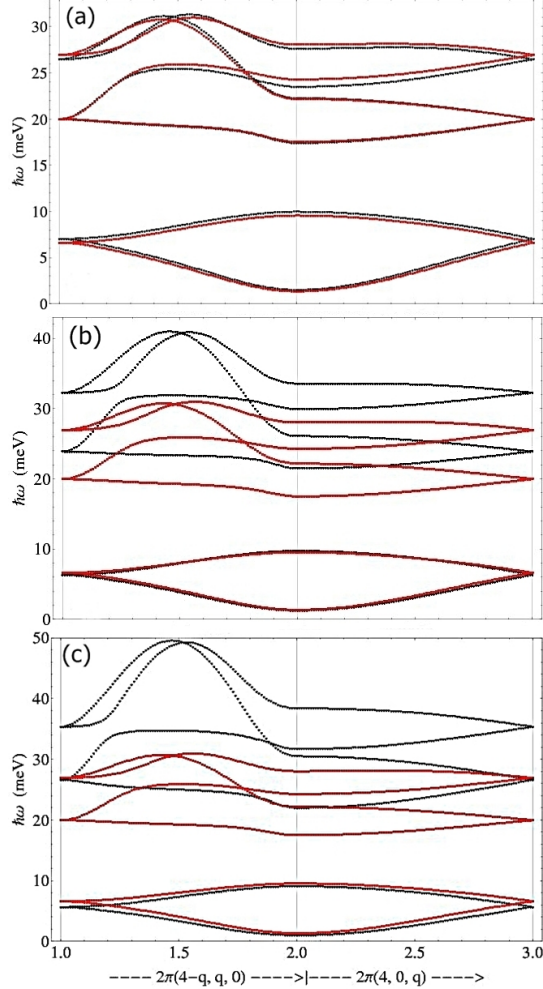


FIG. 6. In all panels, the red lines are experimental and black lines are theoretical spin-waves: (a) Spin wave spectrum for $I4_1/amd$ spin-orbit coupled ferro-orbital order (SOC-FOO) along the high-symmetry lines of the Brillouin zone. We find an excellent match between our theoretical and previous experimental data of Ref. 15. (b) Spin-waves corresponding to the $I4_1/a$ symmetry AFOO I order. The upper four V oscillation branches of the theoretical spin-waves are both too high in energy and have a larger dispersion compared to the experimental plot. (c) Same as in (b), but for the AFOO II order. Here the overestimate in the J_{V-V} is even greater than in (b).

-	CF E_{xy} eV	CF E_{eg} eV	Theory meV	Expt. ¹⁵ meV
Mn D^z	-0.016	1.0	-0.1123	-0.1024
V $D^{x,y}$	-0.024	0.4	-4.056	-4.04
V D^z	-0.024	0.4	7.34	2.79

TABLE II. Table of calculated anisotropy constants for $V^{3+} 3d^2$ and $Mn^{2+} 3d^5$ atomic shells. The energies of E_{xy} and E_{eg} due to the crystal-fields are measured with respect to $E_{yz,zx} = 0$ eV.

erable overestimate of V-V exchange) compared to the correct one in Fig. 6(a). Figure 6(b) shows the spin waves for the ‘AFOO I’ order, which is composed of alternating yz and zx *ab* layers along the c axis.

Figure 6(c) shows the spin waves for the ‘AFOO II’, which is composed of real linear combinations of yz and zx orbitals with the relative sign between yz and zx alternating between *ab* layers along the c axis. As Table I shows, this order again gives a considerably greater V-V exchange compared to the experiment and therefore the upper branches are much higher in energy and have a greater dispersion relative to the experimental plot.

We conclude that the excellent agreement between our theoretical and experimental spin-wave dispersions for all the six oscillation modes can be obtained only when using the exchange interactions derived from the SOC ferro-orbital order with $I4_1/amd$ symmetry, where the second t_{2g} electron occupies a complex linear combination of $|yz\rangle \pm i|zx\rangle$ uniformly on all V-sites. The other two orbital orders, ‘AFOO I’ and ‘AFOO II’, do not give such a good match with experiment throughout the Brillouin Zone, so these orders can be ruled out. We further note that the spin-orbit coupling plays an important role in the orbital physics of V-atoms in MnV_2O_4 . This is also justified by the fact that the single-ion anisotropy is relatively high, as evidenced by the large gaps for the would-be acoustic modes at Γ .

IV. CONCLUSION

By theoretical computations of the interatomic exchange constants using LSDA+U method, magnetic force

theorem and by imposing various orbital ordering scenarios we have shown that the orbital order on the V sites of MnV_2O_4 is similar to a complex linear combination of zx and yz on all V sites. Our calculated spin wave spectra for this order come closest to the experimental data. Further support in an evidence of the complex order is the strong single-ion anisotropy experienced by the spin moments on the V sites. We also predict, based on our $U = 5$ eV, orbital-ordered band-structures, that the low- T phase of MnV_2O_4 is a Mott-type insulator,

and that a half-metal-to-insulator transition accompanies the simultaneous orbital ordering, structural distortion, and non-collinear moment transitions at $T_S = 53$ K.

Acknowledgements.

The authors acknowledge useful discussions with Myung Joon Han, Rajiv Singh and Nick Curro. The work was supported by DOE SciDAC Grant No. SE-FC02-06ER25793 and by DOE Computational Material Science Network (CMSN) Grant No. DE-SC0005468.

-
- ¹ Y. Tokura and N. Nagaosa, *Science* **288**, 462, (2000).
 - ² R. Plumier and M. Sougi, *Solid State Commun.* **64**, 53 (1987); *Physica B* **155**, 315 (1989).
 - ³ V. O. Garlea, R. Jin, D. Mandrus, B. Roessli, Q. Huang, M. Miller, A. J. Schultz, and S. E. Nagler, *Phys. Rev. Lett.* **100**, 066404 (2008).
 - ⁴ S. Sarkar, T. Maitra, Roser Valenti, and T. Saha-Dasgupta, *Phys. Rev. Lett.* **102**, 216405 (2009).
 - ⁵ M. Tinkham, *Group Theory and Quantum Mechanics*, McGraw-Hill, New York, (1964).
 - ⁶ H. Tsunetsugu and Y. Motome, *Phys. Rev. B* **68**, 060405(R) (2003).
 - ⁷ T. Suzuki, M. Katsumura, K. Taniguchi, T. Arima, and T. Katsufuji, *Phys. Rev. Lett.* **98**, 127203 (2007).
 - ⁸ K. Adachi, T. Suzuki, K. Kato, K. Osaka, M. Takata, and T. Katsufuji, *Phys. Rev. Lett.* **95**, 197202 (2005).
 - ⁹ O. Tchernyshyov, *Phys. Rev. Lett.* **93**, 157206 (2004).
 - ¹⁰ K. I. Kugel and D. I. Khomskii, *Sov. Phys.-JETP* **37**, 725 (1973); *Sov. Phys. Usp.* **25**(4), 231 (1982).
 - ¹¹ H. A. Jahn and E. Teller, *Proc. R. Soc. A* **161**, 200 (1937).
 - ¹² For a review, see, e.g., *Theory of the Inhomogeneous Electron Gas*, edited by S. Lundqvist and S. H. March (Plenum, New York, 1983).
 - ¹³ For a review, see, e.g., *Strong Correlations in electronic structure calculations*, edited by V. I. Anisimov (Gordon and Breach Science Publishers, Amsterdam, 2000).
 - ¹⁴ O. K. Andersen, T. Saha-Dasgupta, *Phys. Rev. B* **62**, 16219, (2000).
 - ¹⁵ J.-H. Chung, J.-H. Kim, S.-H. Lee, T. J. Sato, T. Suzuki, M. Katsumura, and T. Katsufuji, *Phys. Rev. B* **77**, 054412 (2008).
 - ¹⁶ D. Alders, R. Coehoorn, W. J. M. de Jonge, *Phys. Rev. B* **63**, 054407 (2001).
 - ¹⁷ J. B. Goodenough, *Magnetism and the Chemical Bond* (Interscience, New York, 1963); J. Kanamori, *J. Phys. Chem. Solids* **10**, 87 (1959).
 - ¹⁸ S.-H. Baek, N. J. Curro, K.-Y. Choi, A. P. Reyes, P. L. Kuhns, H. D. Zhou, and C. R. Wiebe, *Phys. Rev. B* **80**, 140406(R) (2009).
 - ¹⁹ Gia-Wei Chern, Natalia Perkins, and Zhihao Hao, *Phys. Rev. B* **81**, 125127 (2010).
 - ²⁰ O. K. Andersen, *Phys. Rev. B* **12**, 3060 (1975).
 - ²¹ S. Y. Savrasov, *Phys. Rev. B* **54**, 16470 (1996).
 - ²² A. I. Liechtenstein, M. I. Katsnelson, V. P. Antropov, and V. A. Gubanov, *J. Magn. Magn. Mater.* **67**, 65 (1987).
 - ²³ X. Wan, Q. Yin, and S. Y. Savrasov, *Phys. Rev. Lett.* **97**, 266403 (2006).
 - ²⁴ V. I. Anisimov, F. Aryasetiawan, and A. I. Liechtenstein, *J. Phys. Condens. Matter* **9**, 767 (1997).
 - ²⁵ D. I. Khomskii and T. Mizokawa, *Phys. Rev. Lett.* **94**, 156402 (2005).
 - ²⁶ R. Nanguneri, Ph.D. thesis, (2012).
 - ²⁷ T. Miyake and F. Aryasetiawan, *Phys. Rev. B* **77**, 085122 (2008).
 - ²⁸ A. Kokalj, *Comp. Mater. Sci.*, **2003**, Vol. 28, p. 155.